Title: Loss of circulating CD8α$^+$ NK cells during human *Mycobacterium tuberculosis* infection

Authors: Nezar Mehanna[1, †], Atul Pradhan[1,†], Rimanpreet Kaur[1,†], Theodota Kontopoulos[2], Barbra Rosati[1], David Carlson[1], Nai-Kong Cheung[2], Hong Xu[2], James Bean[2], Katherine Hsu[2], Jean-Benoit Le Luduec[2, ‡], and Charles Vorkas[1,3,4‡]

Affiliations:

[1]Renaissance School of Medicine at Stony Brook University, Stony Brook, NY, 11794

[2]Sloan Kettering Institute, Memorial Sloan Kettering Cancer Center, New York, NY 10065

[3]Department of Microbiology and Immunology, Stony Brook University, Stony Brook, NY 11794

[4]Center for Infectious Diseases, Stony Brook University, Stony Brook, NY, 11794

†, ‡: These authors contributed equally to this manuscript.

*Corresponding author Charles Kyriakos Vorkas, MD, charles.vorkas@stonybrookmedicine.edu, 101 Nicolls Road, Health Sciences Center 15060-I, Stony Brook, NY 11794.

Abstract: Natural Killer (NK) cells can recognize and kill *Mtb*-infected cells in vitro, however their role after natural human exposure has not been well-studied. To identify *Mtb*-responsive NK cell populations, we analyzed the peripheral blood of healthy household contacts of active Tuberculosis (TB) cases and source community donors in an endemic region of Port-au-Prince, Haiti by flow cytometry. We observed higher CD8α expression on NK cells in putative resistors (IGRA- contacts) with a progressive loss of these circulating cells during household-associated latent infection and disease. In vitro assays and CITE-seq analysis of CD8α$^+$ NK cells demonstrated enhanced maturity, cytotoxic gene expression, and response to cytokine stimulation

22 relative to CD8α$^-$ NK cells. CD8α$^+$ NK cells also displayed dynamic surface expression dependent
23 on MHC I in contrast to conventional CD8$^+$ T cells. Together, these results support a specialized
24 role for CD8α$^+$ NK cell populations during *Mtb* infection correlating with disease resistance.

25 **Main Text:**

26 **INTRODUCTION**

27 Tuberculosis (TB) remains the leading global cause of death from a single bacterial infection and
28 is a significant public health concern (*1, 2*). Exposure to *Mycobacterium tuberculosis* (*Mtb*) bacilli
29 can result in a broad spectrum of clinical outcomes ranging from clearance of primary infection,
30 asymptomatic latent TB infection (LTBI)—measured by *Mtb* peptide-specific interferon γ release
31 assay (IGRA)—or symptomatic active pulmonary TB disease (*2*). It is estimated that 25% of the
32 global population has evidence of latent infection and 10% will progress to active pulmonary
33 disease (*3*). The host immunologic determinants of these clinical outcomes remain poorly defined
34 and are a major obstacle to designing effective TB vaccines and host-directed therapies to prevent
35 disease. Most TB immunology studies focus on conventional peptide-specific T cells (*4-8*), but
36 the presence of these cells have not been shown to correlate with protection (*9-14*). In contrast,
37 few studies have examined *Mtb*-reactive innate lymphocytes that contribute to *Mtb* clearance (*15-*
38 *18*).

39 Here, we focus on the most abundant innate lymphocytes in mammals: Natural Killer (NK) cells
40 (*19*). NK cells are prevalent in the peripheral blood (0.1-18% of leukocytes) and populate tissue
41 sites such as liver, lung, and mucosal barriers (*20*). They express a broad range of germ-line
42 encoded pattern recognition receptors enabling rapid responses to infection without the need for
43 antigen-specific expansion (*21*). Prior work provides mechanistic evidence for NK cell recognition

44 of intracellular and extracellular *Mtb* in vitro through natural cytotoxicity receptor engagement of
45 *Mtb* cell wall components or stress-induced self-ligands (*22-33*). However, few published studies
46 directly examine NK cell biology during natural *Mtb* transmission in humans (*27, 28, 34*).

47 In this study, we interrogate peripheral blood NK cells in a cohort of household TB contacts in an
48 endemic region in Port-au-Prince, Haiti. We analyzed samples from active TB cases (n=50) and
49 their contacts from the same households (n=50) in addition to interferon-gamma (IFNγ) release
50 assay (IGRA)-matched unrelated donors from the source community without household exposure
51 (n=50). We used spectral flow cytometry to test our hypothesis that specific NK cell
52 subpopulations are activated and expand during household-associated *Mtb* exposure and infection.
53 We identify preserved frequency of CD8α^+ NK cells in blood of uninfected household contacts
54 (IGRA$^-$) with progressive loss of this population during household latent infection and active TB
55 disease. CD8α^+ NK cells demonstrated enhanced responsiveness to cytokine stimulation in vitro
56 compared to CD8α^- NK cells and exhibited dynamic surface expression in culture and after in
57 vitro stimulation. Cellular indexing of transcriptomes and epitopes (CITEseq) revealed largely
58 overlapping transcriptional programs between CD8$\alpha^{+/-}$ NK cells with enhanced expression of
59 select cytotoxicity-associated genes in the CD8α^+ subset. We also observed ubiquitous
60 intracellular NK cell CD8α protein expression. Taken together, our results identify a novel
61 subpopulation of *Mtb*-reactive CD8α^+ NK cells associated with resistance to primary tuberculosis
62 infection.

63 **RESULTS**

64 **Clinical cohort description:**

65 To study early events during the immune response to *Mtb*, we used biobanked samples from a
66 cross-sectional study performed at GHESKIO Centers, Port-au-Prince, Haiti to assemble a clinical
67 cohort of household contacts of active pulmonary TB cases between 2015-2018 (NIH U19
68 AI111143, completed). Out of the total 92 household contacts and 591 community controls
69 enrolled, we randomly sampled an age-, sex-, and IGRA-matched subset of 50 TB household
70 contacts and 50 active TB cases from the same households, as well as 50 source community
71 controls without household exposure, based on peripheral blood mononuclear cell (PBMC)
72 availability and quality control (total N=150). All available specimens from IGRA- contacts were
73 analyzed.

74 Age, sex, IGRA status, and relevant sociodemographic variables are summarized in Table 1. No
75 significant variations were observed in the number of household members, household income,
76 smoking status, or alcohol consumption between groups, consistent with previous work (*15*). Fifty
77 percent of contacts slept in the same room as the active pulmonary TB index case. In the overall
78 study cohort, there were a 50% prevalence of IGRA-positivity in the community controls relative
79 to 75% in contacts, consistent with increased transmission within the household. Among the eleven
80 IGRA- contacts enrolled, only 2 IGRA conversions were detected during 6-month follow-up IGRA
81 testing.

82 **IGRA+ community controls have elevated frequency of mature CD56^{-} NK cells:**

83 We first assessed the frequency of NK cell subpopulations in the clinical cohorts using flow
84 cytometry. Human NK cells were defined by the absence of lineage markers for T cells (CD3),
85 monocytes (CD14), and B cells (CD19), and gated on surface expression of neural cell adhesion
86 molecule (NCAM), CD56, and Fc receptor γRIIIA, CD16 (**Fig. 1A**). We stratified NK cells into
87 three subsets based on expression of CD56: CD56^{-}, CD56^{dim}, and CD56^{bright} (*35, 36*). There was

88 no difference in frequency of total NK cells or CD56^{dim} NK cells between clinical groups (**Fig. 1B**
89 **and 1C center**). IGRA+ community controls had fewer CD56^{bright} NK cells (3.11% vs 5.45%,
90 p=0.006) and more CD56^{-} NK cells (19.1% vs 12.6%, p=0.002) compared to IGRA- controls or
91 IGRA+ contacts, indicating an accumulation of mature NK cells during latent TB infection within
92 the source community **(Fig. 1C, right and left)**.

93 **IGRA+ contacts demonstrate a loss of circulating CD16^{+} NK cells:**

94 NK cell activity against *Mtb* depends upon complex combinatory signaling transduced by
95 activating and inhibiting receptors (*37-39*). We next investigated markers of NK cell activation ex
96 vivo. We analyzed representative receptors, including CD16a (FcγRIIIA), which binds the F_c
97 region of antibodies and can induce antibody-dependent cellular cytotoxicity (ADCC). Within the
98 major CD56^{dim} subset, IGRA+ contacts had decreased circulating CD16^{+} NK cells compared to
99 IGRA+ controls (60% vs 80%, $p < 0.0001$) with a reciprocal increase in CD16^{-} population,
100 representing downregulation or shedding of CD16 surface expression during household-associated
101 LTBI **(Fig. 2A)** (*40*). We found no significant differences in other canonical markers of NK cell
102 activation ex vivo including activation markers CD69 or CD25, or HLA-E restricted receptor
103 NKG2C. We observed decreased staining for degranulation marker CD107a in CD56^{bright} NK cells
104 of IGRA- contacts, potentially representing recent activation events during household exposure.
105 (**Fig. 2B - D**).

106 **NK cells of IGRA- contacts have a depressed functional phenotype:**

107 To assess functional activity of NK cells in vitro, we cultured PBMCs in media alone or with K562
108 cells—a leukemia cell line with low levels of HLA I expression known to activate NK cells—co-
109 incubated at 1:20 K562:PBMC for 15 hours. Cells were then stained, and percent difference was
110 calculated for CD69, CD107a, CD16, and NKG2C. Our positive control analyses in **Fig. 3A**

111 display results from the major CD56^{dim} subset and demonstrate CD107a, CD69, and NKG2C were
112 significantly increased with K562, while CD16 was significantly decreased, across all clinical
113 groups.

114 Next, we directly compared NK cell response to K562 between clinical groups. IGRA+ contacts
115 demonstrated significantly more degranulation (CD107a) and NKG2C expression after
116 stimulation relative to IGRA- contacts (**Fig. 3B, left)**. IGRA+ contacts also demonstrated
117 depressed CD69 responses relative to IGRA+ controls (**Fig. 3B, top right**). No significant
118 differences in CD16 expression were detected. The same analyses applied to CD56^{-} and CD56^{bright}
119 NK cells demonstrated similar responses to stimulation, but no significant differences between
120 clinical groups (**Fig. S1, A - D**). Taken together with our ex vivo data, these in vitro restimulation
121 results indicate that CD56^{dim} NK cells of putative *Mtb* resistors (IGRA- contacts) have depressed
122 function, potentially representing sequelae of recent household-associated *Mtb* exposure.

123 **Loss of circulating CD8α^{+} NK cells during household-associated Mtb infection:**

124 Despite their canonical classification as short-lived innate lymphocytes, NK cells are increasingly
125 recognized for their marked diversity and ability to differentiate into longer-lived effectors (*16,*
126 *18, 27, 41-44*), including after mycobacterial stimuli (*45*). The most extensively studied is an NK
127 cell memory population co-expressing NKG2C and CD57 that expands in blood during human
128 cytomegalovirus (CMV) infection (*27, 46*). Multiple putative markers of NK cell memory during
129 *Mtb* infection have been suggested, including CD57, CD8α, CD161, and CD27 (*28, 34, 45*). We
130 compared expression of these markers across clinical groups and found that household-associated
131 LTBI (IGRA+ contacts) and active TB disease donors had progressively decreasing frequency of
132 CD8α^{+}CD56^{dim} NK cells (**Fig. 4A)**. A similar trend was observed with the marker of terminal
133 differentiation, CD57. There was significantly fewer CD57^{+}CD56^{dim} NK cells in household-

134 associated LTBI (IGRA+ contacts) compared to healthy household contacts (**Fig. 4B**). There was
135 no association between CD8α expression and age or sex, and loss of CD8α$^+$ was specific to NK
136 cells and was not observed among T cells during active TB (**Fig. S2A-B**). We did not observe any
137 significant differences in the expression of CD27, CD127, or CD161 between clinical groups (**Fig**
138 **S3**). Together, these results indicate that donors who develop household-associated LTBI and
139 active TB disease experience a loss of circulating CD8α$^+$ and CD57$^+$ CD56^{dim} NK cells. In turn,
140 CD8α$^+$ NK cell frequency significantly correlates with resistance to primary household-associated
141 infection.

142 **CD8α$^+$ NK cells represent a mature population with high functional potential:**

143 Despite the identification of cytotoxic CD8α$^+$ NK cells over 30 years ago (*47-49*), the function of
144 CD8α on NK cells during health and disease is not well-characterized and is of emerging interest
145 as a cellular target against immune-mediated diseases (*47, 49, 50*). We next used flow cytometry
146 to define co-expressed receptors of CD8α$^+$ NK cells in our cohorts. In the Haitian cohorts, a mean
147 of 27% of NK cells expressed CD8α on their surface. Among NK cell subsets, CD56^{dim} NK cells
148 had the largest proportion of CD8 positivity (median: 36%, range: 1-74%) (**Fig. S4A**). We then
149 defined co-expressed receptors on CD8α$^+$ NK cells among all healthy Haitian donors, excluding
150 active TB cases with chronic symptomatic disease. CD8α$^+$ NK cells expressed significantly higher
151 levels of CD57 and CD16, and lower levels of CD25 and CD127 (**Fig. 4C**). This indicates that
152 CD8α$^+$ NK cells represent more mature effectors compared to their CD8α$^-$ counterparts. When
153 compared to T cells, median fluorescence intensity (MFI) of CD8α surface expression was
154 significantly lower in NK cells (**Fig. S4B**).

155 To interrogate function, PBMCs were co-incubated with K562 cells for 15 hours and compared to
156 resting conditions as described above, stratified by CD8α. CD8α$^+$ NK cells were more responsive
157 to K562 induction measured by CD69 upregulation compared to CD8α$^-$ NK cells but demonstrated
158 lower levels of degranulation as measured by CD107a staining (**Fig. 4D**). The propensity for
159 CD8α$^+$ NK cells to upregulate CD69 upon K562 stimulation was more pronounced among the
160 CD56$^-$ compartment, where the CD8α$^-$ fraction had little to no response (**Fig. 4E**). Overall, this
161 suggests that CD8α expression among NK cells marks a population with higher capacity for
162 activation, specifically among terminally differentiated CD56$^-$ NK cells, that are reported to have
163 depressed effector functions (*51*).

164 **CD8α is ubiquitously expressed in NK cells:**

165 We next interrogated the immune phenotype and function of CD8α$^+$ NK cells in a distinct
166 biorepository of healthy human PBMCs (IRB2021-00478; PI: Vorkas) to validate our findings and
167 perform additional functional assays. First, we confirmed the presence of CD8α expression in NK
168 cells by extracellular staining with CD8α and CD8β antibodies. About 60% of NK cells did not
169 express surface CD8, CD8αα was found in ~40% of NK cells, while rare CD8αβ NK cells were
170 detected (**Fig. 5A**). In blood, CD8α was expressed in all three compartments of NK cells, and most
171 frequently among CD56^{dim} cells, with median expression comparable to Haitian donors (**Fig. 5B**).
172 We also validated our prior result from the contact cohort (**Fig. 4C**) demonstrating CD16 and
173 CD8α were significantly co-expressed (**Fig. 5C).** As our TB contact studies only assessed surface
174 CD8α on NK cells, we next analyzed intracellular CD8α expression by flow cytometry. We
175 observed that nearly all CD56^{dim} NK cells expressed CD8α protein intracellularly, contrasting with
176 T cells whose CD8 expression did not significantly differ between surface and intracellular

177 staining (**Fig. 5D**). CD56^{bright} and CD56^{-} NK cells also demonstrated ubiquitous expression of
178 CD8α protein intracellularly (**Fig. S5**). To test the stability of surface CD8α on NK cells over time,
179 we incubated PBMCs for 1 or 7 days in pro-survival cytokine IL-2. We observed significantly
180 increased CD8α surface expression following prolonged incubation, indicating that surface
181 presentation of NK cell CD8α is more dynamic than in T cells where it is a constitutively expressed
182 surface receptor (**Fig. 5E**).

183 **CD8α^{+} NK cells have enhanced responses to cytokine stimulation:**

184 We next hypothesized that surface CD8α was associated with enhanced responsiveness to
185 inflammatory signals, following prior reports of increased cytotoxicity against leukemic cells
186 relative to CD8α^{-} NK cells (*48*). We stimulated PBMCs with either the potent IL15-IL15Rα sushi
187 domain fusion construct (IL15-15RαSu) (*52*), IL15-15RαSu/IL12/IL18, IL12/IL18 alone, or
188 virulent *Mtb* Erdman whole cell lysate and assessed intracellular IFNγ expression by flow
189 cytometry. Cytokine stimulation led to decreased CD8α^{+} surface staining while *Mtb* stimulation
190 did not alter CD8 surface expression, suggesting that cytokine stimulation induces downregulation
191 of the CD8α receptor or cell death (**Fig. 6A**). Both IL15/IL12/IL18 and to a lesser degree *Mtb*
192 lysate conditions induced IFNγ responses in CD56^{dim} NK cells compared to resting (**Fig. 6B**).
193 When stratified by CD8α, we observed increased intracellular IFNγ with cytokine stimulation in
194 both CD16$^{-/+}$ CD8α^{+} NK cells relative to CD8α^{-} cells, but no differences upon co-incubation with
195 *Mtb* lysates (**Fig. 6C**). Percentage of CD25, CD69, and intracellular Granzyme B responses were
196 also enhanced in CD8α^{+} NK cells across CD56-stratified subsets (**Fig. S6**).

197 **CD8α^{+} surface expression on NK cells is MHC I-dependent:**

198 To determine a mechanism by which CD8α may modulate NK cell function, we hypothesized that
199 CD8α may engage MHC I molecules like $CD8^+$ T cells (*53, 54*). To test this, we stimulated whole
200 PBMCs with MHC I blocking antibody (clone: W6/32) and measured surface CD8α expression.
201 Strikingly, surface CD8α expression on NK cells—but not T cells—was significantly decreased
202 in all anti-MHC I conditions (**Fig. 6D**). Our results indicate that CD8α surface expression is
203 maintained through engagement of MHC I molecules.

204 **$CD8\alpha^+$ NK cells have overlapping transcriptomes with $CD8\alpha^-$ NK cells:**

205 While CD8α-expressing NK cells have previously been described (*47-49, 55*), the transcriptional
206 programs associated with surface expression of CD8α and whether these relate to homologous
207 function in $CD8\alpha^+$ T cells during disease is an area of emerging interest. To interrogate the
208 transcriptional profile of $CD8\alpha^+$ NK cells, we sorted innate lymphocyte subsets from PBMCs
209 including NK cells, γδ T cells, MAIT cells, and invariant Natural Killer T cells (iNKTs) by
210 fluorescence-activated cell sorting (FACS) from the peripheral blood of two healthy donors. We
211 performed CITE-seq (*7*) of these populations directly after sorting or after coincubation for seven
212 days in IL2/IL7 supplemented media +/- *Mtb* lysates in order to define surface protein and
213 transcript expression in CD8α NK cells. We discriminated NK cells from surrounding innate
214 lymphocytes based on surface antibody barcodes for CD56 and CD16 together with expression of
215 canonical NK cell gene transcripts *CD3E*, *NCR1*, and *NCAM1* (CD56) (**Fig. S7**) (*47, 56, 57*).
216 Dimensionality reduction with UMAP identified four clusters of NK cells with distinct
217 transcriptional signatures (**Fig. 7, A to D**). To assess pathogen-specific responses, we first
218 performed differential expression between the 'rest' and '*Mtb* lysate' conditions and display the
219 top 8 most differentially expression genes in **Fig. 7E**. The cytotoxic serine protease *GZMB*

220 *(*Granzyme B*)* and killer immunoglobulin-like receptor, *KIR3DL1*, were the most upregulated
221 genes in the *Mtb* lysate condition.

222 We next analyzed the distribution of *CD8A* transcript and CD8α protein expression among NK
223 cells using both transcript and surface antibody barcodes for CD8α. NK cells did not cluster
224 independently based on the presence of *CD8A*/CD8α (**Fig. 8, F and G**) and *CD8A*$^+$/CD8α$^+$ NK
225 cells were distributed throughout all clusters (**Fig. 8I)**. Low amplification of surface antibody
226 barcodes for CD8α was observed in NK cells, in contrast with other CD8α -expressing immune
227 subsets sequenced (e.g., MAIT cells; **Fig. S8**) in line with CD8α MFI differences detected by flow
228 cytometry (**Fig. S4B**).

229 To define transcriptional signatures associated with *CD8A* transcript expression, we stratified NK
230 cells expressing greater than zero *CD8A* transcripts and performed differential expression relative
231 to *CD8A*$^-$ cells. Half of all NK cells expressed *CD8A* transcripts (**Fig. 8J**). Differential gene
232 expression revealed few statistically significant differences between *CD8A*$^{+/-}$ cells. Notable
233 differentially expressed genes in *CD8A*$^+$ NK cells include cytotoxicity-associated proteins natural
234 cytotoxicity receptor 3 (*NCR3*) and the serine protease granzyme M (*GZMM*) (**Fig. 8K**).

235 **DISCUSSION**

236 Identifying the correlates of protection against natural *Mtb* infection is an area of critical
237 importance that will inform the next generation of TB vaccines and host-directed therapies (*5, 37,*
238 *45, 58-61*). In this study, we hypothesized that investigation of household-associated *Mtb* exposure
239 would reveal specialized NK cell populations and represent early events following high-risk
240 transmission. Our results identify a CD8α-expressing NK cell subpopulation with preserved
241 frequency in the blood of contacts who remain uninfected (IGRA-) that is progressively depleted
242 during household LTBI and active TB disease. Few studies have interrogated CD8α$^+$ NK cells, as

243 this receptor is most commonly understood as a lineage marker for T cells (*62*) and is absent in
244 specific pathogen free murine NK cells (*63*). Recent work reporting an association of CD8α^{+} NK
245 cells with protection against human infectious, autoinflammatory and malignant disease has
246 generated interest in targeting this subpopulation for host-directed therapeutics (*39, 47, 48*).
247 However, little is known how CD8α receptors may modulate NK cell activity, namely, enhanced
248 cytotoxic functions previously reported in vitro against leukemia cells and strong associations with
249 protection against both infectious and non-infectious diseases. (*48, 50, 55*). Here, we show that the
250 majority of peripheral blood NK cells can express CD8α protein, but neither *CD8A* transcript nor
251 CD8α protein marked a distinct transcriptional state in healthy donors. Importantly, we
252 demonstrate that surface expression of CD8α on NK cells depends upon MHC I expression and
253 marks a population with enhanced responsiveness to cytokine stimuli in vitro. Together, our study
254 highlights a novel innate effector against human tuberculosis and provides important insights into
255 NK cell biology and innate TB immunology.

256 To our knowledge, there have been only two published household TB contact studies that
257 specifically examined NK cell biology during early *Mtb* exposure and infection. Our study expands
258 upon the sample size of this prior work and provides additional analyses of NK cell subpopulations
259 stratified by CD56 not previously addressed (*42, 64, 65*). Specifically, we observed decreased
260 frequency of immature CD56^{bright} NK cells with reciprocal increase in mature CD56^{-} NK cells
261 during community LTBI, in line with findings during chronic viral infections such hepatitis C and
262 HIV (*66-68*). We also observed that CD16 expression was increased during community LTBI
263 relative to household-associated infection, which may represent a late effect of latency within the
264 CD56^{dim} subset (*61*). An equally valid interpretation of these results is that loss of surface CD16
265 is an early event detected after household-associated exposure and may represent downregulation

266 or shedding of the $F_c\gamma$ receptor after engagement (*40*). Together, these changes in frequency of
267 CD16 and CD56 expression indicate a gradual expansion of mature NK cells in peripheral blood
268 after asymptomatic infection (*29, 40, 64, 65, 67, 69*), accompanied by both markers of maturity
269 and dysfunction (loss of CD56), but also enhanced potential for ADCC (gain of CD16).

270 Two phenotypic markers whose surface expression were both independently and inversely
271 associated with infection in households, were CD8α and CD57. CD8α has long been appreciated
272 to be expressed on the surface of human (*47-50, 70*) and non-human primate NK cells (*63, 71*).
273 CD8α expression on human NK cells has been associated with enhanced cytotoxicity (*48, 55*) and
274 is referred to in one study as a putative *Mtb* memory marker (*45*). Recent studies in prospective
275 longitudinal human cohorts report that loss of CD8α expression at the transcript (*CD8A*) or protein
276 level correlate with HIV progression (*39, 49*), relapsing multiple sclerosis (*47*), and recurrence of
277 acute myeloid leukemia after stem cell transplantation (*50*), where $CD8\alpha^+$ NK cells are
278 hypothesized to exercise combined cytotoxic and regulatory roles to prevent disease. Sorted
279 surface $CD8\alpha^+$ NK cells also demonstrate enhanced anti-leukemia cytotoxicity in vitro compared
280 to sorted $CD8\alpha^-$ cells (*50*). We also report that $CD8\alpha^+$ NK cells were prevalent in healthy US
281 donors with ubiquitous intracellular CD8α protein expression. This finding suggests that most NK
282 cells are capable of presenting CD8α to the cell surface to enhance effector function, in contrast
283 to constitutive surface CD8α expression on T cells. Moreover, $CD8\alpha^+$ NK cells were exquisitely
284 sensitive to cytokine stimulation, suggesting complex roles during inflammatory immune
285 responses against disease. Further, we show that CD8α surface expression was strongly dependent
286 on MHC I expression (*50, 54, 72*) raising critical questions for future studies to define the
287 molecular mechanisms of CD8α engagement with MHC I and to determine whether this may be

288 modulated by different peptide-MHC I complexes. Taken together with previously published work
289 (*47-49*), CD8α$^+$ NK cell subpopulations emerge as an attractive target in vaccination and host-
290 directed approaches against infectious and noninfectious diseases (*73*).

291 In addition to these mechanistic insights, we present the first multi-omic analysis of CD8α$^+$ NK
292 cells and show that in contrast to T cells, CD8α does not mark a distinct transcriptional state of
293 NK cells in healthy donors assayed, though *CD8A*$^+$ NK cells did differentially express cytotoxic
294 genes including *NCR3* and *GZMM*. These results will need to be validated in other healthy donors
295 as well as compared to future CITE-seq experiments in high-risk *Mtb* exposure cohorts or other
296 disease states.

297 There are certain limitations inherent to our human immunology study design. While household
298 contacts experienced high risk exposures to pre-treatment smear+ active TB cases, this does not
299 exclude the possibility they may have been exposed or infected in the community. We control for
300 this using source community donors to account for background transmission. Similarly, IGRA-
301 community controls may have also been recently exposed and resisted primary infection, though
302 this group represents the most rigorous control for household exposure. Our study was conducted
303 in one TB endemic population in Haiti and will need to be validated in other cohorts. Due to the
304 largely cross-sectional study design, we were unable to follow study volunteers beyond 6 months
305 for IGRA- contacts, of whom only two converted to IGRA+ providing insufficient sample size to
306 analyze correlates of IGRA conversion prospectively. Finally, all our biological samples in TB
307 cohorts were derived from human blood and may not represent the abundance or function of NK
308 cells within infected lung tissue. Future studies in *Mtb*-infected donors with multi-omic validation
309 are needed to understand the role of CD8α$^+$ NK cells at primary sites of infection.

310 In sum, our study adds to the growing literature highlighting a protective role for CD8α^+ NK cells
311 against both infections and non-infectious immune-mediated disease. Ongoing work will define
312 how surface CD8$\alpha\alpha^+$ NK cells may enhance targeting of *Mtb*-infected cells and will inform future
313 cellular therapies and vaccination approaches to prevent or treat TB disease.

314 **MATERIALS AND METHODS**

315 **Study design and participant recruitment:**

316 *Donor recruitment and protection of human subjects.* Haitian donors were enrolled through the
317 Tri-Institutional Tuberculosis Research Unit (TBRU) at the Groupe Haitien d'etude du Sarcome
318 de Kaposi et des Infections Opportunistes (GHESKIO) Centers under Institutional Review Board
319 Approval at Weill Cornell Medicine and GHESKIO Centers in Haiti. All participants provided
320 written informed consent, including consent for future use of biobanked samples for research. A
321 dedicated clinical field team at the GHESKIO Centers in Port-au-Prince, Haiti, recruited as part of
322 the NIH-funded TBRU (AI111143). LTBI was detected using QuantiFERON-TB® Gold
323 (QIAGEN), and active TB was excluded by clinical screening for signs and symptoms of active
324 TB including fever, cough, night sweats, weight loss, and abnormal findings on Chest X-ray. Most
325 contacts were recruited close to the time of diagnosis of the index case and were living in the same
326 house as the active TB case for at least 1 month in the 6 months prior to diagnosis (median time to
327 contact recruitment from TB case diagnosis, 2.4 months; range, 0.2-26 months). To select for high
328 transmission settings, each household was required to have a history of two active pulmonary TB
329 cases. Healthy donors without reported TB exposure from the same community were recruited as
330 controls. All cases with active pulmonary TB received periodic follow-up appointments while on
331 treatment, and anyone with known contact with an active TB patient who remained IGRA-
332 received 6-month follow-up and was rescreened with IGRA. The median smear grade of the active

333 pulmonary TB cases in the households was 2-3+, conferring high risk for person-to-person
334 transmission (*74*). All donors provided informed consent prior to peripheral blood donation for
335 PBMC isolation. All donor samples were de-identified on site using a barcode system before they
336 were shipped to Stony Brook University for analysis. Healthy donors were also recruited at Stony
337 Brook University (SBU) under IRB2021-00478 (PI: Vorkas) and New York Blood Center
338 (NYBC), which were used for stimulation assays and CITE-seq.

339 **PBMC isolation:**

340 PBMCs were isolated from peripheral blood at GHESKIO (Port-au-Prince, Haiti) using the Ficoll-
341 Paque (GE Healthcare) density centrifugation, frozen in 5×10^6 cells/ml aliquots in 90% FBS/10%
342 DMSO (Thermo Fisher Scientific) and stored at –80°C prior to being shipped on dry ice to New
343 York. PBMCs from healthy donors recruited at SBU and New York Blood Center (NYBC) were
344 isolated using Ficoll-Paque, BD Vacutainer CPT cell preparation tube (Becton, Dickinson and
345 Company) or SepMate tubes (Stem Cell Technologies) using the manufacturer protocol. PBMCs
346 isolated at SBU were cryopreserved in serum free Bambanker medium (GC Lymphotec) and stored
347 in liquid N_2.

348 **Flow cytometry acquisition and analysis:**

349 A complete list of fluorescent antibodies is listed in Supplementary Table 1: Reagents and
350 resources. All antibodies were commercially acquired, and multicolor panels were designed and
351 validated using fluorescent minus one (FMO) controls. MR1 tetramers were obtained from the
352 NIH Tetramer Core Facility (Atlanta, GA). In brief, cryopreserved PBMCs were thawed, plated,
353 Fc receptor blocked (eBioscience), and underwent direct ex vivo extracellular staining for 15
354 minutes at room temperature (RT). For intracellular staining, PBMCs were incubated with 1X
355 Brefeldin A (BioLegend) for final hour of incubation prior to staining with intracellular antibodies.

356 Samples were then washed twice with FACS buffer and acquired using an Aurora Spectral
357 Analyzer (Cytek). Flow cytometry analysis, including manual gating, was performed using FCS
358 Express 7 (De Novo Software) or R (v4.3.1) with the following library packages downloaded from
359 Bioconductor: *flowWorkspace, ggcyto, and flowCore*.

360 ***Mtb* whole cell lysate:**

361 *Mtb* whole cell lysate was prepared in Biosafety Level 3 facility at SBU. Fifty mL of *Mtb* Erdman
362 7H9 culture was grown to OD_{600} 0.6, centrifuged at 4000 × g for 10 min at RT and pellet was
363 resuspended in 2.5 ml of 10mM Tris-HCl buffer (pH 7.5) and rotated for 2 hr at RT. The mixture
364 was centrifuged at 500 × g for 15 min at RT and aqueous phase was collected and filtered twice
365 through 0.22 µM spin filter (Corning Costar Spin-X) at 6000 × g for 5 min. The aliquots were
366 stored at -80°C for further use.

367 **NK cell co-culture with K562 cell line**

368 K562 cells (ATCC) were incubated in Iscove's Modified Dulbecco's Medium (IMDM)
369 supplemented with 10% FBS. Cryopreserved K562 cells were thawed at 37°C water bath and cells
370 were cultured at 1 x 10^5 viable cells/ml in T-75 flask as per manufacturers protocol. Once the cell
371 density reached 1 x 10^6 cells/ml, K562 was co-incubated with PBMCs at 1:20 K562 to PBMC in
372 a round bottom clear plate (Greiner) for 15 hrs, at 37°C with 5% CO_2. At the beginning of
373 incubation period anti-CD107a antibody was added to the culture. After incubation was complete,
374 cells were washed, stained and acquired by flow cytometry.

375 **NK cell stimulation assay:**

376 Cryopreserved healthy donor PBMCs from SBU and NYBC were used for NK cell stimulation
377 assays. Thawed PBMCs were cultured 1 x 10^4 cells per well in round bottom clear plate (Greiner)

378 for 15 hr, at 37°C with 5% CO_2. Samples were stimulated and incubated overnight in complete
379 RPMI media with 10% heat-inactivated FBS and supplemented with IL-2 (50 U/ml; PeproTech).
380 The cytokine stimulation conditions were performed with commercially available recombinant IL-
381 12 (100 ng/mL; BioLegend), recombinant IL-18 (100 ng/mL; Biolegend) and IL15-Su construct
382 (1 µg/ml) containing a truncated Sushi domain of IL15Rα synthesized by the Cheung lab, that is
383 demonstrated to be a more potent and stable compound with longer half-life than recombinant
384 IL15 (*52*). For *Mtb* stimulation condition we used 1:100 and 1:200 dilution of *Mtb* whole cell
385 lysate.

386 **MHC I blockade:**

387 Cryopreserved healthy donor PBMCs from SBU and NYBC were used for MHC I blockade.
388 PBMCs were thawed at 37°C and incubated in complete RPMI media with 10% heat-inactivated
389 FBS and supplemented with IL-2 (50 U/ml; PeproTech). 1 x 10^4 PBMCs were plated per well in
390 round bottom clear plate (Greiner) and incubated with or without 5 µg/ml *Invivo*MAb anti-human
391 MHC I (clone W6/32; Bio X cell) for 15 hr, at 37°C with 5% CO_2 before being stained and
392 acquired.

393 **scRNA-seq and CITE-seq library generation and sequencing:**

394 PBMCs were stained with fluorescent antibodies for cell sorting of MAIT cells ($CD3^+$, $CD161^+$,
395 MR1-5-OP-RU $tetramer^+$), NK cells ($CD3^-$, $CD19^-$, $CD14^-$, $CD16^+$ $CD56^{dim}$), γδ T cells ($CD3^+$,
396 $TCR\gamma\delta^+$) and iNKT cells ($CD161^+$ $iNKT^+$) using FACS. The sorted cells were blocked with human
397 Trustain, FcX blocking reagent (BioLegend) for 10 minutes at 4°C and then stained with TotalSeq-
398 C barcoded tagged and hashtags antibodies for 30 minutes at 4°C in a total volume of 100ul. The
399 residual TotalSeq-C and hashtags antibodies were removed by centrifugation at 400 *g* for 5

400 minutes at 4ºC. A complete hashtag and TotalSeq-C antibody list is provided in **Supplementary**
401 **Table 1: Reagent and Resources.**

402 Gene expression and surface antigen library preparation was conducted at the Stony Brook
403 University Single Cell Genomics Facility. Briefly, cell viability and concentrations were
404 determined on a Countess 3FL with trypan blue staining. Approximately 5,000 live cells from each
405 condition were loaded in a single 10X Genomics 5' NextGEM Single Cell assay reaction (30,000
406 total cells per reaction), to perform 5' single cell immune profiling assay using a Chromium iX
407 instrument (10X Genomics). Gene expression (GEX) and surface antigen (SA) libraries were
408 prepared, and quality controlled using Chromium NextGEM 5' Single Cell with Feature Barcode
409 assay and a TapeStation 4200, according to the manufacturer's instructions. The libraries were
410 sequenced at a depth of approx. 25,000 (GEX) and 10,000 (SA) paired reads/cell on an Illumina
411 NovaSeqX sequencer (Novogene, Inc).

412 The gene expression and surface feature barcode raw FASTQ files of single cell RNA-seq were
413 analyzed on Cell Ranger (10x Genomics, v.7.0) (https://www.10xgenomics.com/analysis-
414 guides/demultiplexing-and-analyzing-5%E2%80%99-immune-profiling-libraries-pooled-with-
415 hashtags), multi-pipeline with human reference transcriptome (GRCh38) downloaded from 10x
416 Genomics website and hashtag configuration file, which contained the barcodes related to each
417 different samples.

418 **Single-cell RNAseq analysis:**

419 The generated gene expression matrix files were analyzed with R (4.3.2) using the *Seurat* (5.0)
420 package and cells were filtered based on following criteria: 1.) the number of genes was equal to
421 or greater than 200 and below than 6000 and 2.) the mitochondrial percentage was less than 5.
422 Using the FindVariableFeatures() function we selected the top 3000 features with highest variance.

423 Then, different samples were integrated using the harmony algorithm and scaled. Log-
424 normalization and principal component analysis (PCA) was done on integrated values. The top 20
425 principal components were selected for clustering and visualization with UMAP using the default
426 Louvain algorithm. Differential gene expression was performed using FindAllMarkers() with a
427 minimum threshold of 25% cells expressing.

428 **Statistical Analysis:**

429 Statistical analysis was performed using R (4.3.2) and GraphPad Prism (10.1.2). Non-parametric
430 testing with Wilcoxon tests was used to compare the means between groups for flow markers. P-
431 values were not adjusted because cross-wise comparisons were not performed between all six
432 clinical groups. Only comparisons a priori hypothesized to represent biological features were
433 tested, these included: IGRA- contacts vs controls, IGRA+ contacts vs controls, IGRA- contact vs
434 IGRA+ control, and IGRA+ control vs Active TB.

435 **Supplementary Materials**

436 Supplementary Table 1: Reagents and resources. See attached file.

437 **References and Notes:**

438 1. R. M. Houben, P. J. Dodd, The Global Burden of Latent Tuberculosis Infection: A Re-
439 estimation Using Mathematical Modelling. *PLoS Med* **13**, e1002152 (2016).

440 2. S. Bagcchi, WHO's Global Tuberculosis Report 2022. *Lancet Microbe* **4**, e20 (2023).

441 3. K. M. Shea, J. S. Kammerer, C. A. Winston, T. R. Navin, C. R. Horsburgh, Jr., Estimated
442 rate of reactivation of latent tuberculosis infection in the United States, overall and by
443 population subgroup. *Am J Epidemiol* **179**, 216-225 (2014).

444 4. K. B. Urdahl, S. Shafiani, J. D. Ernst, Initiation and regulation of T-cell responses in
445 tuberculosis. *Mucosal Immunol* **4**, 288-293 (2011).
446 5. E. Nemes *et al.*, Prevention of M. tuberculosis Infection with H4:IC31 Vaccine or BCG
447 Revaccination. *N Engl J Med* **379**, 138-149 (2018).
448 6. D. R. Tait *et al.*, Final Analysis of a Trial of M72/AS01E Vaccine to Prevent Tuberculosis.
449 *N Engl J Med* **381**, 2429-2439 (2019).
450 7. A. Nathan *et al.*, Multimodally profiling memory T cells from a tuberculosis cohort
451 identifies cell state associations with demographics, environment and disease. *Nat Immunol*
452 **22**, 781-793 (2021).
453 8. A. Pradhan, C. K. Vorkas, T cells target TB. *Cell Host Microbe* **31**, 329-330 (2023).
454 9. A. M. Gallegos *et al.*, A gamma interferon independent mechanism of CD4 T cell mediated
455 control of M. tuberculosis infection in vivo. *PLoS Pathog.* **7**, e1002052 (2011).
456 10. S. Sakai *et al.*, CD4 T Cell-Derived IFN-gamma Plays a Minimal Role in Control of
457 Pulmonary Mycobacterium tuberculosis Infection and Must Be Actively Repressed by PD-
458 1 to Prevent Lethal Disease. *PLoS Pathog.* **12**, (2016).
459 11. H. A. Fletcher, L. Schrager, TB vaccine development and the End TB Strategy: importance
460 and current status. *Trans R Soc Trop Med Hyg* **110**, 212-218 (2016).
461 12. G. Voss *et al.*, Progress and challenges in TB vaccine development. *F1000Res* **7**, 199
462 (2018).
463 13. J. D. Ernst, Mechanisms of M. tuberculosis Immune Evasion as Challenges to TB Vaccine
464 Design. *Cell Host Microbe* **24**, 34-42 (2018).
465 14. D. Roordink *et al.*, The TB vaccine development pathway - An innovative approach to
466 accelerating global TB vaccine development. *Tuberculosis (Edinb)* **126**, 102040 (2021).

467 15. C. K. Vorkas *et al.*, Mucosal-associated invariant and gammadelta T cell subsets respond
468 to initial Mycobacterium tuberculosis infection. *JCI Insight* **3**, (2018).
469 16. J. A. Choreno-Parra, L. I. Weinstein, E. J. Yunis, J. Zuniga, R. Hernandez-Pando, Thinking
470 Outside the Box: Innate- and B Cell-Memory Responses as Novel Protective Mechanisms
471 Against Tuberculosis. *Front Immunol* **11**, 226 (2020).
472 17. S. A. Khader *et al.*, Targeting innate immunity for tuberculosis vaccination. *J Clin Invest*
473 **129**, 3482-3491 (2019).
474 18. J. A. Choreño Parra *et al.*, Memory of Natural Killer Cells: A New Chance against
475 Mycobacterium tuberculosis? *Front Immunol* **8**, 967 (2017).
476 19. D. Artis, H. Spits, The biology of innate lymphoid cells. *Nature* **517**, 293-301 (2015).
477 20. P. Dogra *et al.*, Tissue Determinants of Human NK Cell Development, Function, and
478 Residence. *Cell* **180**, 749-763.e713 (2020).
479 21. L. L. Lanier, Natural killer cell receptor signaling. *Current opinion in immunology* **15**, 308-
480 314 (2003).
481 22. P. Schierloh *et al.*, Mycobacterium tuberculosis-induced gamma interferon production by
482 natural killer cells requires cross talk with antigen-presenting cells involving Toll-like
483 receptors 2 and 4 and the mannose receptor in tuberculous pleurisy. *Infect Immun* **75**, 5325-
484 5337 (2007).
485 23. S. Venkatasubramanian *et al.*, IL-21-dependent expansion of memory-like NK cells
486 enhances protective immune responses against Mycobacterium tuberculosis. *Mucosal*
487 *Immunol* **10**, 1031-1042 (2017).
488 24. S. Esin, G. Batoni, Natural killer cells: a coherent model for their functional role in
489 Mycobacterium tuberculosis infection. *J Innate Immun* **7**, 11-24 (2015).

490 25. C. B. W. Giacoia-Gripp *et al.*, Changes in the NK Cell Repertoire Related to Initiation of
491 TB Treatment and Onset of Immune Reconstitution Inflammatory Syndrome in TB/HIV
492 Co-infected Patients in Rio de Janeiro, Brazil-ANRS 12274. *Front Immunol* **10**, 1800
493 (2019).
494 26. M. Allen *et al.*, Mechanisms of Control of Mycobacterium tuberculosis by NK Cells: Role
495 of Glutathione. *Front Immunol* **6**, 508 (2015).
496 27. M. Garand *et al.*, Functional and Phenotypic Changes of Natural Killer Cells in Whole
497 Blood during Mycobacterium tuberculosis Infection and Disease. *Front Immunol* **9**, 257
498 (2018).
499 28. L. D. Harris *et al.*, Distinct Human NK Cell Phenotypes and Functional Responses to
500 Mycobacterium tuberculosis in Adults From TB Endemic and Non-endemic Regions.
501 *Front Cell Infect Microbiol* **10**, 120 (2020).
502 29. G. Batoni *et al.*, Human CD56bright and CD56dim natural killer cell subsets respond
503 differentially to direct stimulation with Mycobacterium bovis bacillus Calmette-Guérin.
504 *Scand J Immunol* **62**, 498-506 (2005).
505 30. S. Esin *et al.*, Interaction of Mycobacterium tuberculosis cell wall components with the
506 human natural killer cell receptors NKp44 and Toll-like receptor 2. *Scand J Immunol* **77**,
507 460-469 (2013).
508 31. S. Esin *et al.*, Functional characterization of human natural killer cells responding to
509 Mycobacterium bovis bacille Calmette-Guérin. *Immunology* **112**, 143-152 (2004).
510 32. R. Vankayalapati *et al.*, Role of NK cell-activating receptors and their ligands in the lysis
511 of mononuclear phagocytes infected with an intracellular bacterium. *J Immunol* **175**, 4611-
512 4617 (2005).

513 33. R. Vankayalapati *et al.*, The NKp46 receptor contributes to NK cell lysis of mononuclear
514 phagocytes infected with an intracellular bacterium. *J Immunol* **168**, 3451-3457 (2002).
515 34. D. Tripathi *et al.*, Metabolites enhance innate resistance to human Mycobacterium
516 tuberculosis infection. *JCI Insight* **7**, (2022).
517 35. M. E. Ross, M. A. Caligiuri, Cytokine-induced apoptosis of human natural killer cells
518 identifies a novel mechanism to regulate the innate immune response. *Blood* **89**, 910-918
519 (1997).
520 36. W. E. Carson *et al.*, Interleukin (IL) 15 is a novel cytokine that activates human natural
521 killer cells via components of the IL-2 receptor. *J Exp Med* **180**, 1395-1403 (1994).
522 37. S. Suliman *et al.*, Peripheral Blood Mucosal-Associated Invariant T Cells in Tuberculosis
523 Patients and Healthy Mycobacterium tuberculosis-Exposed Controls. *J Infect Dis* **222**, 995-
524 1007 (2020).
525 38. P. Schierloh *et al.*, Increased susceptibility to apoptosis of CD56dimCD16+ NK cells
526 induces the enrichment of IFN-gamma-producing CD56bright cells in tuberculous
527 pleurisy. *J Immunol* **175**, 6852-6860 (2005).
528 39. B. Lucia, C. Jennings, R. Cauda, L. Ortona, A. L. Landay, Evidence of a selective depletion
529 of a CD16+ CD56+ CD8+ natural killer cell subset during HIV infection. *Cytometry* **22**,
530 10-15 (1995).
531 40. K. Srpan *et al.*, Shedding of CD16 disassembles the NK cell immune synapse and boosts
532 serial engagement of target cells. *J Cell Biol* **217**, 3267-3283 (2018).
533 41. I. Terren *et al.*, Cytokine-Induced Memory-Like NK Cells: From the Basics to Clinical
534 Applications. *Front Immunol* **13**, 884648 (2022).

535 42. D. Brownlie *et al.*, Expansions of adaptive-like NK cells with a tissue-resident phenotype
536 in human lung and blood. *Proc Natl Acad Sci U S A* **118**, (2021).
537 43. R. Nikzad *et al.*, Human natural killer cells mediate adaptive immunity to viral antigens.
538 *Sci Immunol* **4**, (2019).
539 44. N. M. Adams *et al.*, Cytomegalovirus Infection Drives Avidity Selection of Natural Killer
540 Cells. *Immunity* **50**, 1381-1390 e1385 (2019).
541 45. S. Suliman *et al.*, Bacillus Calmette-Guérin (BCG) Revaccination of Adults with Latent
542 Mycobacterium tuberculosis Infection Induces Long-Lived BCG-Reactive NK Cell
543 Responses. *J Immunol* **197**, 1100-1110 (2016).
544 46. K. Van Der Ploeg *et al.*, Emergence of Human CMV-induced NKG2C+ NK cells is
545 Associated with CD8+ T cell Recovery following Allogeneic HCT. *Blood Adv*, (2023).
546 47. E. F. McKinney *et al.*, A CD8(+) NK cell transcriptomic signature associated with clinical
547 outcome in relapsing remitting multiple sclerosis. *Nat Commun* **12**, 635 (2021).
548 48. E. G. Addison *et al.*, Ligation of CD8alpha on human natural killer cells prevents
549 activation-induced apoptosis and enhances cytolytic activity. *Immunology* **116**, 354-361
550 (2005).
551 49. F. Ahmad *et al.*, High frequencies of polyfunctional CD8+ NK cells in chronic HIV-1
552 infection are associated with slower disease progression. *J Virol* **88**, 12397-12408 (2014).
553 50. M. W. Lowdell *et al.*, Evidence that continued remission in patients treated for acute
554 leukaemia is dependent upon autologous natural killer cells. *Br J Haematol* **117**, 821-827
555 (2002).
556 51. N. K. Björkström, H.-G. Ljunggren, J. K. Sandberg, CD56 negative NK cells: origin,
557 function, and role in chronic viral disease. *Trends in Immunology* **31**, 401-406 (2010).

558 52. H. Xu, I. N. Buhtoiarov, H. Guo, N. V. Cheung, A novel multimeric IL15/IL15Rα-Fc
559 complex to enhance cancer immunotherapy. *Oncoimmunology* **10**, 1893500 (2021).
560 53. L. J. Walker *et al.*, Human MAIT and CD8alphaalpha cells develop from a pool of type-
561 17 precommitted CD8+ T cells. *Blood* **119**, 422-433 (2012).
562 54. H. Cheroutre, F. Lambolez, Doubting the TCR coreceptor function of CD8alphaalpha.
563 *Immunity* **28**, 149-159 (2008).
564 55. K. Kushima *et al.*, Flow cytometric analysis of chicken NK activity and its use on the effect
565 of restraint stress. *J Vet Med Sci* **65**, 995-1000 (2003).
566 56. M. Gutierrez-Arcelus *et al.*, Lymphocyte innateness defined by transcriptional states
567 reflects a balance between proliferation and effector functions. *Nat Commun.* **10**, 687
568 (2019).
569 57. C. Yang *et al.*, Heterogeneity of human bone marrow and blood natural killer cells defined
570 by single-cell transcriptome. *Nat Commun* **10**, 3931 (2019).
571 58. M. Musvosvi *et al.*, T cell receptor repertoires associated with control and disease
572 progression following Mycobacterium tuberculosis infection. *Nat Med*, (2023).
573 59. S. Suliman *et al.*, MR1-Independent Activation of Human Mucosal-Associated Invariant
574 T Cells by Mycobacteria. *J Immunol.* **203**, 2917-2927 (2019).
575 60. P. Andersen, T. J. Scriba, Moving tuberculosis vaccines from theory to practice. *Nat Rev*
576 *Immunol* **19**, 550-562 (2019).
577 61. R. Roy Chowdhury *et al.*, A multi-cohort study of the immune factors associated with M.
578 tuberculosis infection outcomes. *Nature* **560**, 644-648 (2018).
579 62. D. Masopust, V. Vezys, E. J. Wherry, R. Ahmed, A brief history of CD8 T cells. *Eur J*
580 *Immunol* **37 Suppl 1**, S103-110 (2007).

581 63. L. J. Kieffer *et al.*, Human CD8 alpha expression in NK cells but not cytotoxic T cells of
582 transgenic mice. *Int Immunol* **8**, 1617-1626 (1996).
583 64. B. Muller-Durovic, J. Grahlert, O. P. Devine, A. N. Akbar, C. Hess, CD56-negative NK
584 cells with impaired effector function expand in CMV and EBV co-infected healthy donors
585 with age. *Aging (Albany NY)* **11**, 724-740 (2019).
586 65. A. Poli *et al.*, CD56bright natural killer (NK) cells: an important NK cell subset.
587 *Immunology* **126**, 458-465 (2009).
588 66. A. S. Fauci, D. Mavilio, S. Kottilil, NK cells in HIV infection: paradigm for protection or
589 targets for ambush. *Nat Rev Immunol* **5**, 835-843 (2005).
590 67. N. K. Björkström, H. G. Ljunggren, J. K. Sandberg, CD56 negative NK cells: origin,
591 function, and role in chronic viral disease. *Trends Immunol* **31**, 401-406 (2010).
592 68. B. Rehermann, M. Nascimbeni, Immunology of hepatitis B virus and hepatitis C virus
593 infection. *Nat Rev Immunol* **5**, 215-229 (2005).
594 69. L. L. Lanier, R. Testi, J. Bindl, J. H. Phillips, Identity of Leu-19 (CD56) leukocyte
595 differentiation antigen and neural cell adhesion molecule. *J Exp Med* **169**, 2233-2238
596 (1989).
597 70. L. A. Terry, J. P. DiSanto, T. N. Small, N. Flomenberg, Differential expression and
598 regulation of the human CD8 alpha and CD8 beta chains. *Tissue Antigens* **35**, 82-91 (1990).
599 71. R. L. Webster, R. P. Johnson, Delineation of multiple subpopulations of natural killer cells
600 in rhesus macaques. *Immunology* **115**, 206-214 (2005).
601 72. J. Geng, M. Raghavan, CD8alphaalpha homodimers function as a coreceptor for
602 KIR3DL1. *Proc Natl Acad Sci U S A* **116**, 17951-17956 (2019).

603 73. S. Schmidt, L. Tramsen, B. Rais, E. Ullrich, T. Lehrnbecher, Natural killer cells as a
604 therapeutic tool for infectious diseases - current status and future perspectives. *Oncotarget*
605 **9**, 20891-20907 (2018).
606 74. H. del Corral *et al.*, IFNgamma response to Mycobacterium tuberculosis, risk of infection
607 and disease in household contacts of tuberculosis patients in Colombia. *PLoS One* **4**, e8257
608 (2009).

609 **Acknowledgments:** We are thankful for the support of the Stony Brook Foundation, the
610 Department of Medicine of the Renaissance School of Medicine and the Office of the Vice
611 President of Research of Stony Brook University. We thank Daniel W. Fitzgerald, MD
612 (Weill Cornell Medicine, Center for Global Health) and Michael S. Glickman (Memorial
613 Sloan Kettering Cancer Center) for generously providing clinical samples from TB contact
614 cohorts. We thank Joseph C. Sun (MSKCC) for valuable discussions on adaptive NK cells.
615 We are also grateful to Thomas MacCarthy, PhD (Stony Brook University, Applied
616 Mathematics) for supportive advice regarding CITE-seq analyses, who passed away during
617 the preparation of this manuscript.

618 **Funding:** This study was supported by the Tri-I TBRU, part of the TBRU Network (U19
619 AI11143). CKV acknowledges support from the NIAID T32 Pathogenesis of Infectious
620 Diseases Training Program (T32AI007613-18; Roy Gulick, WCM), the IDSA Education
621 and Research Foundation Postdoctoral Fellowship Award in Infectious Diseases, a Potts
622 Memorial Foundation Award, NIAID K08AI132739, R21AI171578, and R21AI183259.

623 **Author contributions:** The following authors contributed to the manuscript in various ways. Each
624 author's contribution is listed below.

625 Conceptualization: KH, JBL, CKV

Methodology: NKC, AP, RK, KCH, JBL, CKV

Investigation: NM, AP, RK, TK, BR, NKC, HX, JBL and CKV

Visualization: NM, AP, RK, JB, BR, DEC, JBL, and CKV

Funding acquisition: CKV

Writing – original draft: NM, AP, CKV

Writing – review & editing: all authors

Competing interests: Authors declare that they have no competing interests.

Data and materials availability: All data, code, and materials used in the analysis will be available to any researcher for purposes of reproducing or extending the analysis.

636 **Figures:**

Variable	Control (n=50)	Contact (n=50)	Active TB (n=50)
Age – yr	30.1 ± 9.3	33.9 ± 17.8	20.2 ± 4.26
≤ 18 yr	2 (4)	12 (24)	18 (36)
>18 and <65	48 (96)	35 (76)	32 (64)
≥ 65 yr	0 (0)	3	0 (0)
Female sex – no. (%)	26 (52)	30 (60)	26 (52)
IGRA positive – no. (%)	25 (50)	34 (68)	38 (76)

637 **Table 1. Demographics of study participants in Haitian Cohort (N=150)**

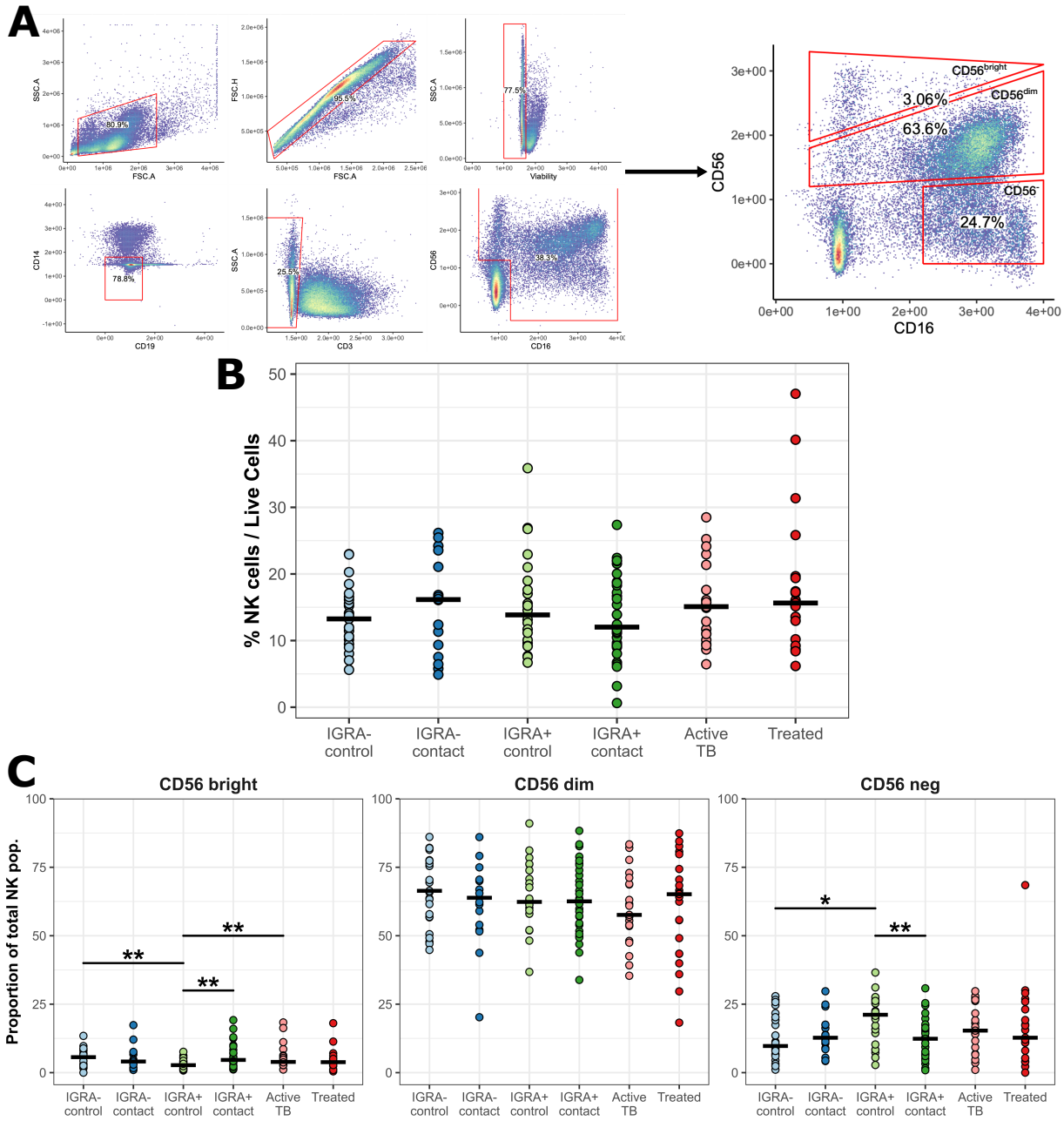

Fig. 1. Frequencies of NK cell subpopulations are altered after *Mtb* infection. **(A)** Gating strategy employed for NK cells from a representative sample. NK cells were defined as CD19$^-$, CD3$^-$, CD14$^-$ lymphocytes who expressed any level of either CD16 or CD56. NK cells were further subdivided into three subsets based on CD56 expression. **(B)** Change in frequency of total NK cells as a proportion of total live population. **(C)** Frequency of each NK cell subset in clinical groups. Frequency calculated as percent of each subset among total NK cells. Brackets represent Wilcoxon statistical tests, with unadjusted p-values. *$p \leq 0.05$, **$p \leq 0.01$.

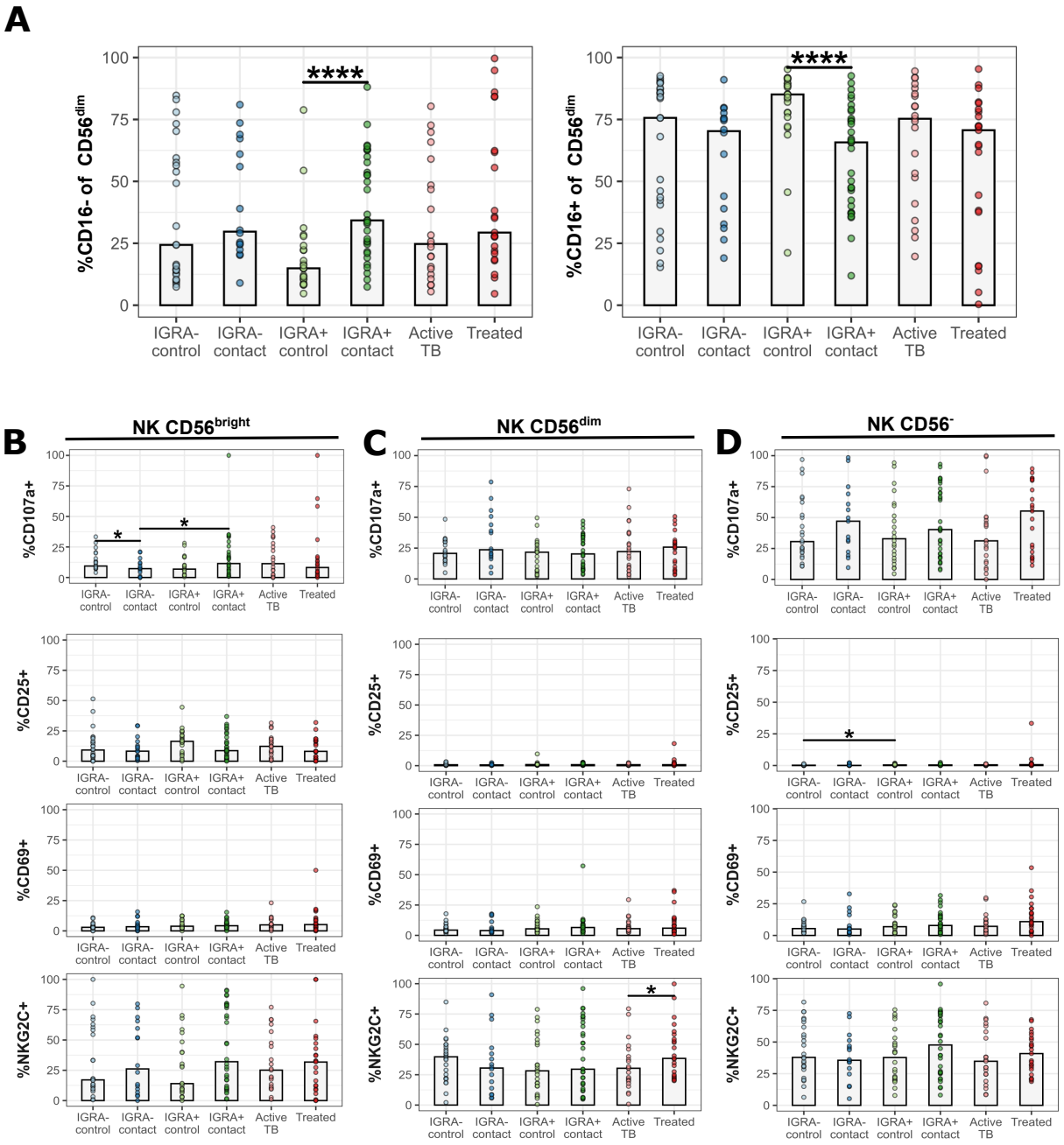

Fig. 2. NK cells demonstrate loss of CD16 expression during household-associated latent infection. (A) Frequency of CD16 in CD56^{dim} NK cells. Brackets represent Wilcoxon tests with unadjusted p-values. Percent positive for 5 activation markers in **(B)** CD56^{bright} NK cells, **(C)** CD56^{dim} NK cells, and **(D)** CD56^{-} NK cells. Brackets represent Wilcoxon tests with unadjusted p-values. *$p \leq 0.05$, ****$p \leq 0.0001$.

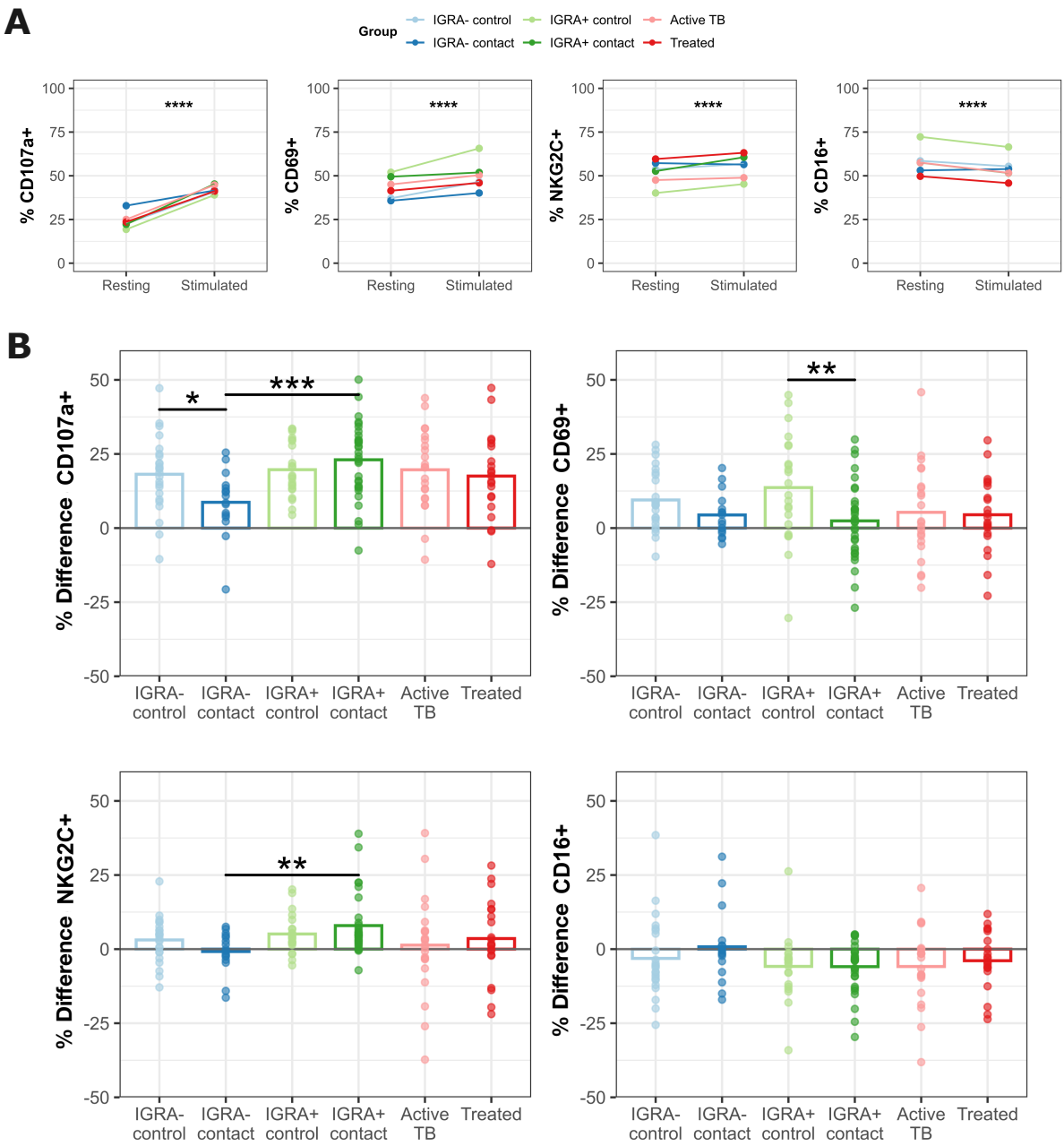

650 **Fig. 3. *Mtb* resistors demonstrate depressed NK cell function in vitro.** NK cells stimulated overnight by co-
651 culture with K562 cell line compared to plain media alone. **(A)** Overall results of activation assay for
652 $CD56^{dim}$ NK cells for four activation markers. Y-axis represents mean percent positive for each activation
653 marker. P values calculated as a global paired Wilcoxon test including all clinical groups. Each clinical
654 group is displayed separately indicated by line color. **(B)** Percent difference of four activation markers
655 (stimulated minus resting) comparing between clinical groups. Brackets represent Wilcoxon tests with
656 unadjusted p-values. *$p \leq 0.05$, **$p \leq 0.01$, ***$p \leq 0.001$, ****$p \leq 0.0001$.

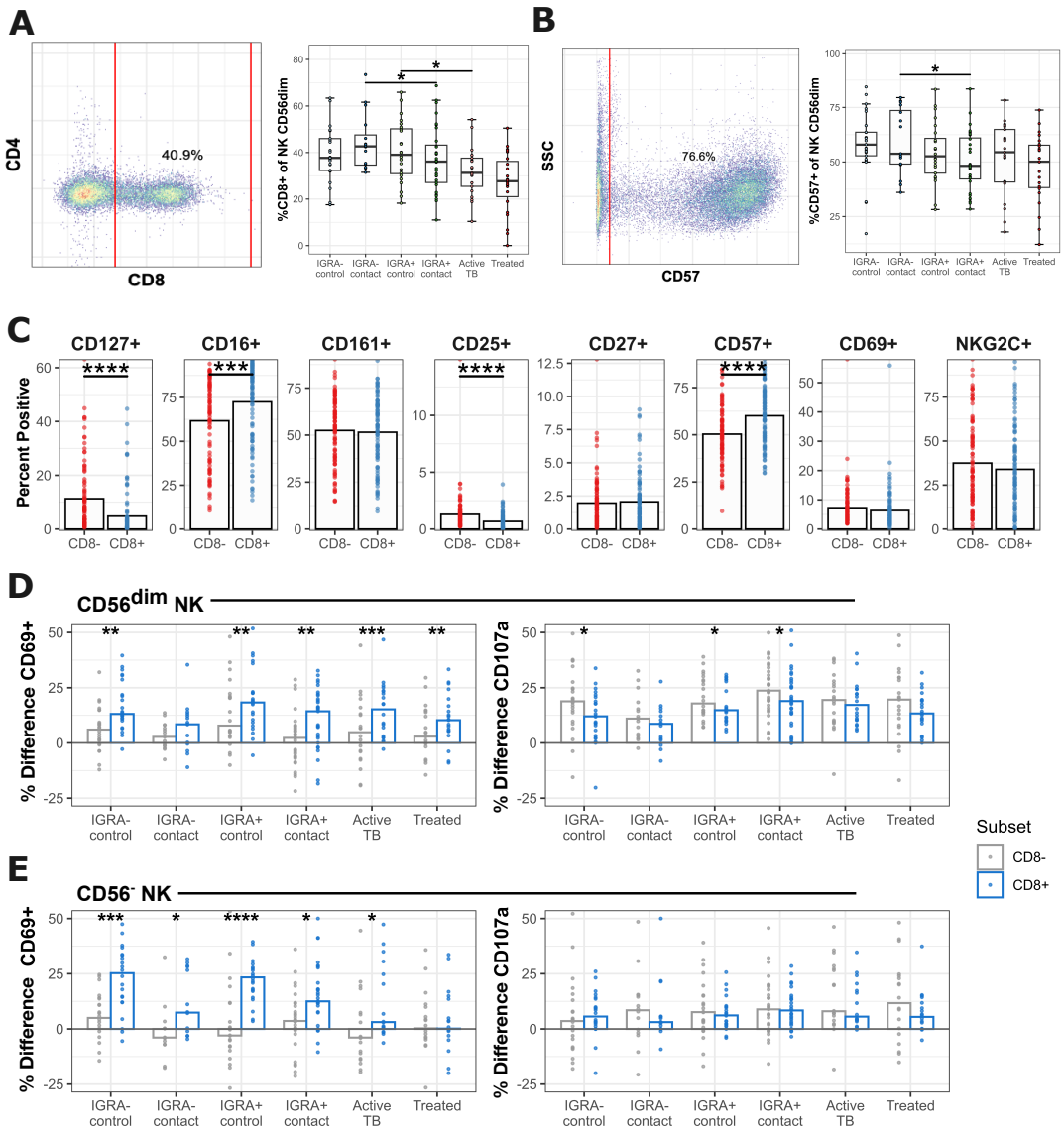

Fig. 4. CD8α⁺ NK cells are depleted in the blood of cases with household-associated *Mtb* infection. (A) Representative gating of CD8α$^+$ in CD56^{dim} NK cells and frequency of CD8α$^+$ within CD56^{dim} NK cells. **(B)** Representative gating of CD57 in CD56^{dim} NK cells and boxplots of percent CD57$^+$ within CD56^{dim} NK cells. **(C)** Expression of select surface markers between CD8α$^+$ vs CD8α$^-$ CD56^{dim} NK cells, active TB are excluded. **(D)** Activation assay with overnight K562 co-culture versus plain media comparing CD8α$^+$ vs CD8α$^-$ CD56^{dim} NK cells. Y-values represent percent difference for CD69 and CD107a. Asterisks represent paired Wilcoxon tests. **(E)** As in panel D, instead displaying CD56$^-$ NK cells. P-values represent unadjusted Wilcoxon testing. *$p \leq 0.05$, **$p \leq 0.01$, ***$p \leq 0.001$, ****$p \leq 0.0001$.

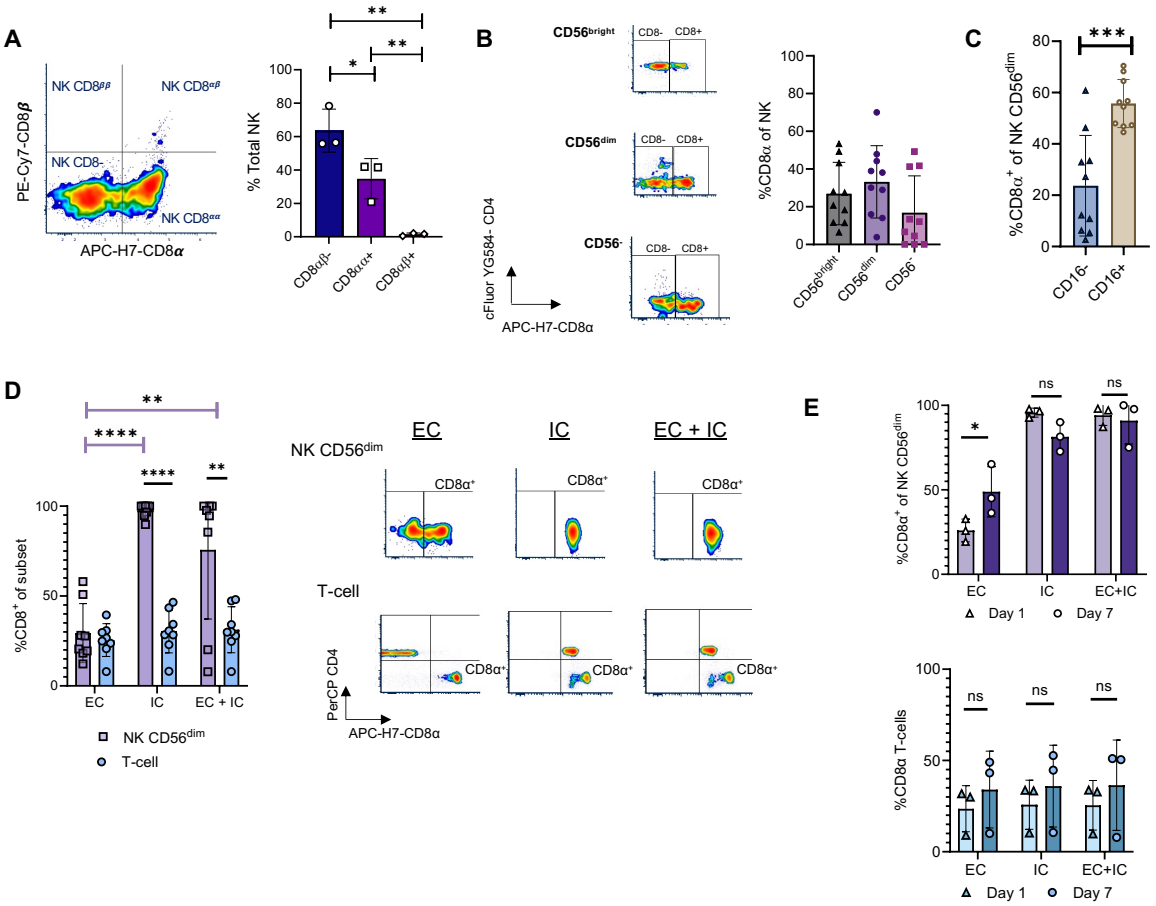

Fig. 5. CD8α$^+$ NK cells are prevalent in healthy US donors with ubiquitous intracellular CD8α expression. **(A)** Flow cytometry plot and percentage of CD8αα$^-$, CD8αα$^+$, CD8αβ$^+$, and CD8ββ$^+$ among total NK (N=3). **(B)** Percentage of CD8α$^+$ NK cells in different subsets based on CD56 expression (N=10). **(C)** Frequency of CD16 expression in CD8α$^+$ CD56^{dim} NK cells. **(D)** Frequency and representative flow cytometry plots of CD8α expression comparing CD56^{dim} NK cells and T cells with extracellular (EC), IC (Intracellular), and EC + IC CD8α staining. **(E)** Percent CD8α$^+$ in EC, IC, and EC + IC staining at day 1 and day 7 in CD56^{dim} NK cells and T cells. Statistical significance was measured using unpaired t tests, ns – no significance, *p<0.05, **p<0.005, ***p<0.001, ****p<0.0001.

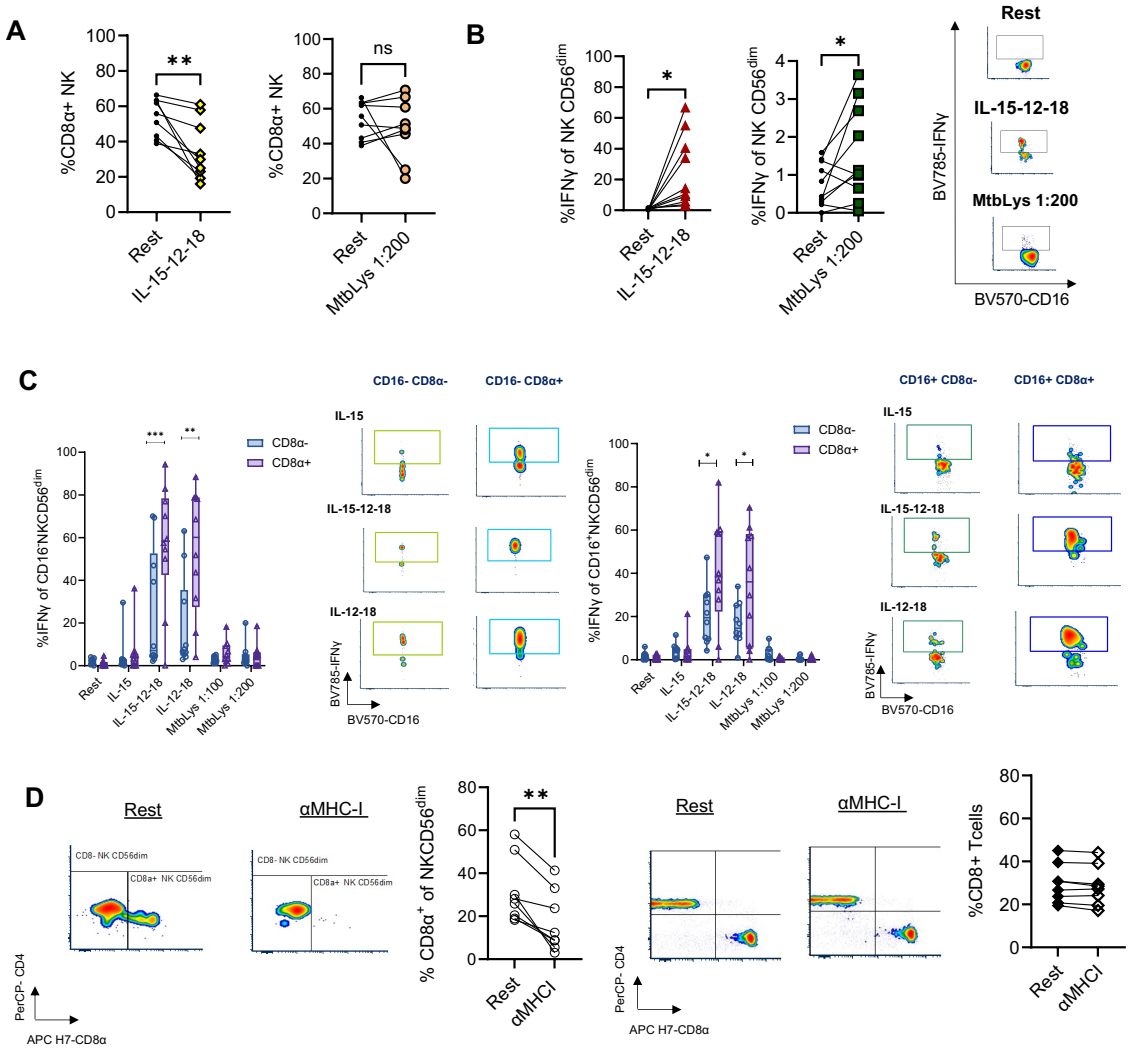

Fig. 6. CD8α$^+$ CD56^{dim} NK cells have enhanced response to cytokine stimulation. (**A**) Pairwise analysis of percent CD8α$^+$ NK cells upon stimulation with IL15/12/18 and MtbLys 1:200 (n=9). (**B**) Pairwise analysis and representative flow plots of intracellular IFNγ in NK CD56^{dim} upon stimulation with IL15/12/18 and MtbLys at dilution 1:200 (n=9). (**C**) Percent intracellular IFNγ$^+$ in CD8α$^+$ versus CD8α$^-$ CD56^{dim} NK cells comparing IL-15-Su, IL15-Su/12/18, IL-12/18, or MtbLys conditions (n=9). Both the CD16$^+$ (right) and CD16$^-$ (left) CD56^{dim} NK subpopulations are displayed. (**D**) Representative flow cytometry plots and paired analysis of percent change CD8α$^+$ with anti-MHC I for 15 hours among CD56^{dim} NK cells (left) and CD8$^+$ T cells (right) (n=8). Statistical significance was measured using paired t-test, with threshold of *p<0.05, **p<0.005, ***p<0.001. IFNγ: Interferon γ, Mtb Lys: *Mtb* whole cell lysate.

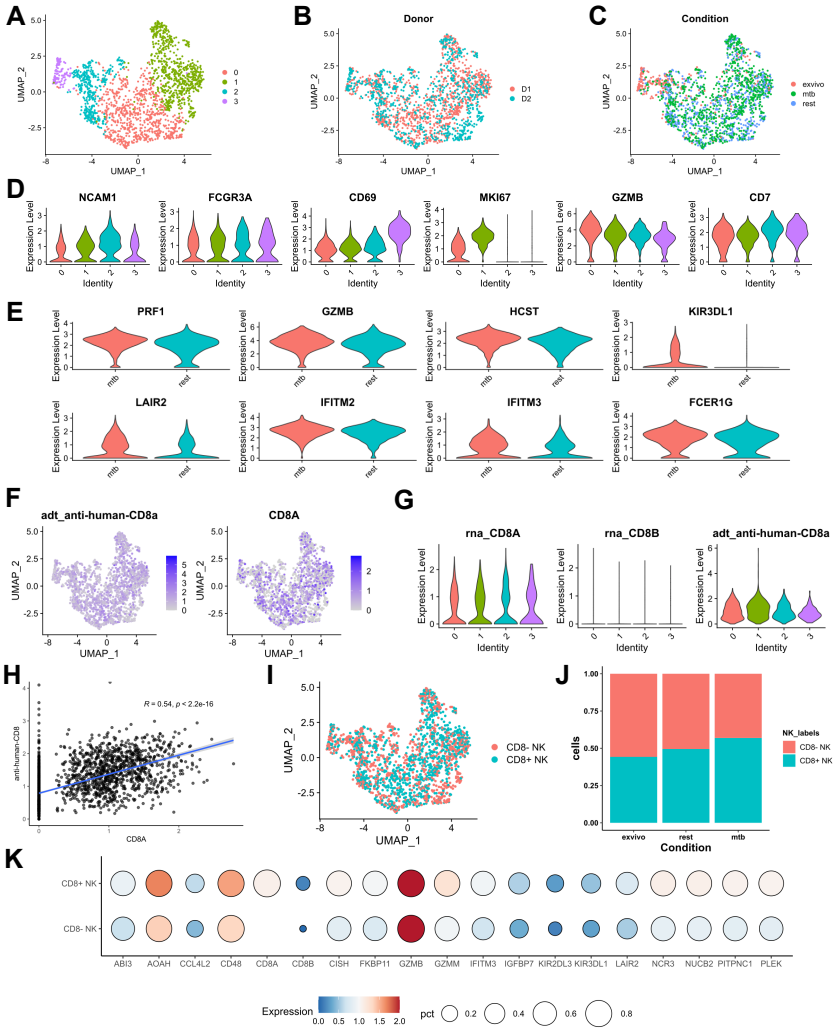

Fig. 7. CITE-seq analysis of CD8α$^+$ vs CD8α$^-$ NK cells from two healthy donors reveals overlapping transcriptomes. (A) Results of clustering and uniform manifold approximation (UMAP) projection for all NK cells. **(B)** UMAP reduction colored by Donor. **(C)** UMAP reduction colored by condition. **(D)** Violin plots representing top six genes that were differentially expressed between the four NK cell clusters. **(E)** Violin plots of the eight differentially expressed genes between resting and *Mtb* lysate condition. **(F)** Distribution of NK cell expression of CD8 based on barcoded antibodies against CD8α and *CD8A* transcript. **(G)** Violin plot of the expression of *CD8A* and *CD8B* transcripts, as well as CD8α surface expression between the four NK cell clusters. **(H)** Correlation of CD8α expression between transcript and protein measurement. **(I)** Annotated UMAP based on transcript expression of *CD8A* into CD8α$^+$ and CD8α$^-$ NK cells. **(J)** Percent of NK cells expressing CD8A transcript between stimulation conditions. **(K)** Dot-plot of genes differentially expressed between CD8α$^+$ and CD8α$^-$ NK cells.